Materials Chemistry and Physics 110 (2008) 471–480

Contents lists available at ScienceDirect

Materials Chemistry and Physics

journal homepage: www.elsevier.com/locate/matchemphys

Studies of interaction of amines with TOPO/TOP capped CdSe quantum dots: Role of crystallite size and oxidation potential

Shailesh N. Sharma [a,*], Himani Sharma [a,b], Gurmeet Singh [b], S.M. Shivaprasad [a]

[a] Electronic Materials Division, National Physical Laboratory, Dr. K. S. Krishnan Marg, New Delhi 110012, India
[b] Department of Chemistry, University of Delhi, Delhi 110007, India

ARTICLE INFO

Article history:
Received 17 March 2007
Received in revised form 23 February 2008
Accepted 29 February 2008

Keywords:
Nanostructures
Photoluminescence spectroscopy
Semiconductors
Fourier transform infrared spectroscopy (FTIR)

ABSTRACT

This work reports the interaction of aliphatic (triethyl amine, butyl amine) and aromatic amines (PPD, aniline) with CdSe quantum dots of varied sizes. The emission properties and lifetime values of CdSe quantum dots were found to be dependent on the oxidation potential of amines and crystallite sizes. Smaller CdSe quantum dots (size ~5 nm) ensure better surface coverage of amines and hence higher quenching efficiency of amines could be realized as compared to larger CdSe quantum dots (size ~14 nm). Heterogeneous quenching of amines due to the presence of accessible and inaccessible set of CdSe fluorophores is indicated. PPD owing to its lowest oxidation potential (~0.26 V) has been found to have higher quenching efficiency as compared to other amines TEA and aniline having oxidation potentials ~0.66 and >1.0 V, respectively. Butyl amine on the other hand, plays a dual role: its post-addition acts as a quencher for smaller and enhances emission for larger CdSe quantum dots, respectively. The beneficial effect of butyl amine in enhancing emission intensity could be attributed to enhance capping effect and better passivation of surface-traps.

1. Introduction

Semiconductor QDs present considerable advantages over bulk single-crystal semiconductors [1]. They have gained increasing attention of scientists and engineers of various disciplines in the past decade due to their flexible processibility and unique properties [2–4]. Owing to their size-dependent fluorescence tunable across the visible spectrum, CdSe QDs have become the most extensively investigated QDs [5]. For a number of optoelectronic applications, e.g., light-emitting diodes (LED) [6,7], strongly luminescent semiconductor nanocrystals are highly desirable. However, due to the large surface-to-volume ratio of nanoparticles, the most common reason for poor luminescence efficiency is non-radiative recombination of light-generated charge carriers at surface-traps [8]. Elimination of these traps can be achieved either by proper chemical modification of the particle surface [9,10] or by growing hetero-epitaxially an inorganic passivation shell around the semiconductor cores [11,12].

CdSe nanocrystals stabilized by TOP/TOPO groups are colloidally stable in a range of nonpolar organic solvents [13]. The sterically bulky and weakly bound TOP/TOPO species are readily substituted by a variety of other ligand molecules like amines [14]. According to Kamat and coworkers [14], direct interaction between the CdSe surface and amine functional groups passivates the surface and blocks the trapping of electrons at the defect sites. Lisensky et al. [15] studied interactions between monoamines or diamines and n-type CdSe substrates. They found that EDA (ethylenediamine) could reversibly enhance the band-edge photoluminescence intensity of single-crystal CdSe. On the other hand, for TOPO-capped CdSe nanocrystals, El-Sayed and coworkers [4] report a decreased emission yield at high concentrations of butyl amine with no specific change in the emission decay lifetime. These researchers attributed the quenching behavior to the electron-donating property of *n*-butyl amine [4]. Kamat and Chandrasekharan [16] reported an enhancement in the emission efficiency by a factor of two for CdSe colloids prepared by reverse micelles upon its surface functionalization with triethyl amine. Since the oxidation potential of amines vary over a wide range, their interaction with CdSe can produce different results. Moreover, nanoparticle stability has not been studied quantitatively and the effect of particle size and capping agent on the photodegradation of CdSe nanocrystals remains largely unexplored. In this work, we have further assessed the role of surface-bound species by selecting aliphatic (triethyl amine) as well as aromatic amine (aniline) with varied oxidation potentials in order to probe the interaction between amines and CdSe nanocrystals. This study provides insight into the quenching mechanism of various amines at the CdSe particle surface. Such knowledge is potentially of great use in designing both light emitters based on

* Corresponding author.
E-mail address: shailesh@mail.nplindia.ernet.in (S.N. Sharma).

0254-0584/$ – see front matter © 2008 Elsevier B.V. All rights reserved.
doi:10.1016/j.matchemphys.2008.02.038

CdSe nanoparticles, where quenching must be avoided, and chemical detectors, where fluorescence quenching is a potential detection mechanism.

2. Experimental

The synthesis of CdSe nanoparticles was carried out by the chemical route using TOP/TOPO capping method to control the growth of the nanoparticles to desired sizes, whose details can be found elsewhere [17,18]. The materials used were of the purest quality available and used as received. Absorption spectra were recorded using Shimadzu 3101 spectrometer. The PL was measured using a home-assembled system consisting of a two-stage monochromator, a photomultiplier tube (PMT) with a lock-in amplifier for PL detection, and an Ar^+ ion laser operating at 488 nm and 5 mW (corresponding to 0.125 W cm^{-2}) power for excitation. Emission lifetime measurements were performed using a laser strobe fluorescence lifetime spectrometer (Photon Technique International). The excitation was carried out using a 337 nm pulsed N_2 laser. Fourier Transform Infrared (FTIR) spectra were recorded with a PerkinElmer Model (Spectrum BX) spectrophotometer.

3. Results and discussion

In a chemical precipitation method, a variety of approaches have been considered to arrest the growth of particles of desired size [16,19]. We employed TOPO capping to arrest the growth of CdSe particles. A change in the ratio of Cd:Se during the precipitation conditions produced particles of different diameters. Different Cd/Se ratios were explored since lower Cd/Se ratios result in the large size particle regime with high quantum yield, whereas, particles produced using higher Cd/Se ratios were found to be of smaller size [16–18]. The crystallite sizes were measured by the blue shift of the absorption edge with respect to bulk CdSe and were found to be ~14.0 and 5.0 nm, respectively. The quantum confinement effect becomes apparent when the semiconductor crystal size is smaller than the bulk Bohr diameter of the CdSe exciton. For CdSe, this value is ~11.2 nm [20]. Different crystallite sizes less or greater than the Bohr diameter of the CdSe exciton were used in order to study the size quantization effects of CdSe nanocrystallites upon its interaction with different amines.

Fig. 1(A and B) depicts the absorption and emission intensity profiles of individual CdSe nanocrystallites of sizes 14 and 5 nm, respectively. In an earlier work, at higher Cd/Se precursor ratio's of ~2:1 and 3:1, it was found that TOPO capped CdSe nanocrystallites (sizes ~5 and 7 nm) exhibited strong quantum size effects [17]. The absorption features of smaller CdSe nanocrystallite (size ~5 nm) suggested monodispersity. However, polydispersity features were evident for larger sized CdSe nanocrystallites (size ~14 nm) corresponding to lower precursor Cd/Se ratio ~0.5:1, respectively.

Fig. 2(a and b) shows the TEM micrographs of CdSe nanocrystals corresponding to Cd:Se precursor ratio's of 0.5:1 and 2:1 while Fig. 2(c and d) represents the corresponding CdSe nanocrystals in the presence of PPD, respectively. As evident from Fig. 2(a) (Cd:Se ~ 0.5:1), the grains are spherically shaped though sparsely populated. The micrograph shows the presence of agglomerated (up to 100 nm in size) as well as dispersed smaller particles. The inset on the left hand side of Fig. 2(a) shows the presence of distinctly visible smaller sized particle (size ~15 nm) even inside the larger clusters. With further increase in Cd/Se ratio from 0.5:1 to 2:1, the micrograph in Fig. 2(b) exhibits a much more compact and dense structure with increasing tendency of agglomeration as compared to the corresponding micrograph of 0.5:1 precursor ratio system. Here, the main features are spherical in shape and exhibit an average size of 40 nm (Fig. 2(b)) which significantly deviates from the particle size of 5 nm as calculated from the absorption edge values. However, magnification of the selected portion of Fig. 2(b) (inset on the left side) reveals that a typical nano sized CdSe growth island is in fact a cluster of several smaller nanocrystals (size ~4–5 nm) each surface passivated by

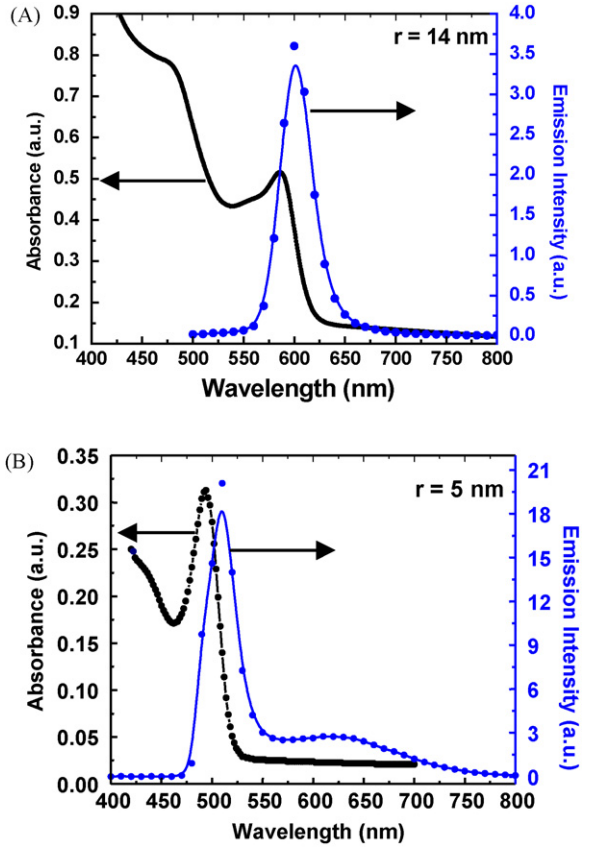

Fig. 1. Absorbance and emission intensity spectra of pure CdSe nanocrystals of size (r) (A) 14 and (B) 5 nm, respectively.

TOP/TOPO groups. Due to extremely small dimensions and high surface energy, these nanocrystallites aggregate to give a resultant average size of 40 nm. However, upon introduction of amine PPD in the CdSe system corresponding to both Cd:Se ~ 0.5:1 and 2:1, although the number density of nanocrystallite increases and the agglomeration tendency is maintained, the resultant crystallite size invariably remains the same (Fig. 2(c) and (d)).

Fig. 3(A and B) shows the comparison of the emission intensity profiles of toluene-suspended CdSe nanocrystallites of varied sizes (5 and 14 nm) as a function of concentration of different amines (PPD, aniline, TEA), respectively. From Fig. 3, it is evident that the emission yield of CdSe system decreases with increase in concentration of amines with rate of quenching in the order of $PL_{quenching}$ (PPD) > $PL_{quenching}$ (TEA) > $PL_{quenching}$ (aniline). In Fig. 3(A and B), it is found that the PPD quenching efficiency in the case of largest CdSe crystallite size ~14 nm is not as efficient as compared to smaller nanocrystallites of size 5 nm. This can be attributed to the fact that 14 nm CdSe nanocrystallite owing to its larger crystallite size imposes steric hindrance and thus less surface coverage of the amines on the CdSe nanocrystallites surface is realized. This hinders the quenching efficiency of PPD for larger CdSe nanocrystallite size (~14 nm) as compared to smaller nanocrystallite size (~5 nm), respectively. The fact that PPD is an effective quencher even at low concentrations particularly for emission of smaller CdSe nanocrystallite (5 nm) suggests that it is capable of directly intercepting one of the charge carriers, thus disrupting the radiative recombination process (reactions (1) and (2)):

$$\mathrm{CdSe} + h\nu \rightarrow \mathrm{CdSe}(h + e) \rightarrow \mathrm{CdSe} + h\nu' \quad (1)$$

$$\mathrm{CdSe}(h) + \mathrm{PPD} \rightarrow \mathrm{CdSe} + \left[\mathrm{PPD}\right]^{+} \quad (2)$$

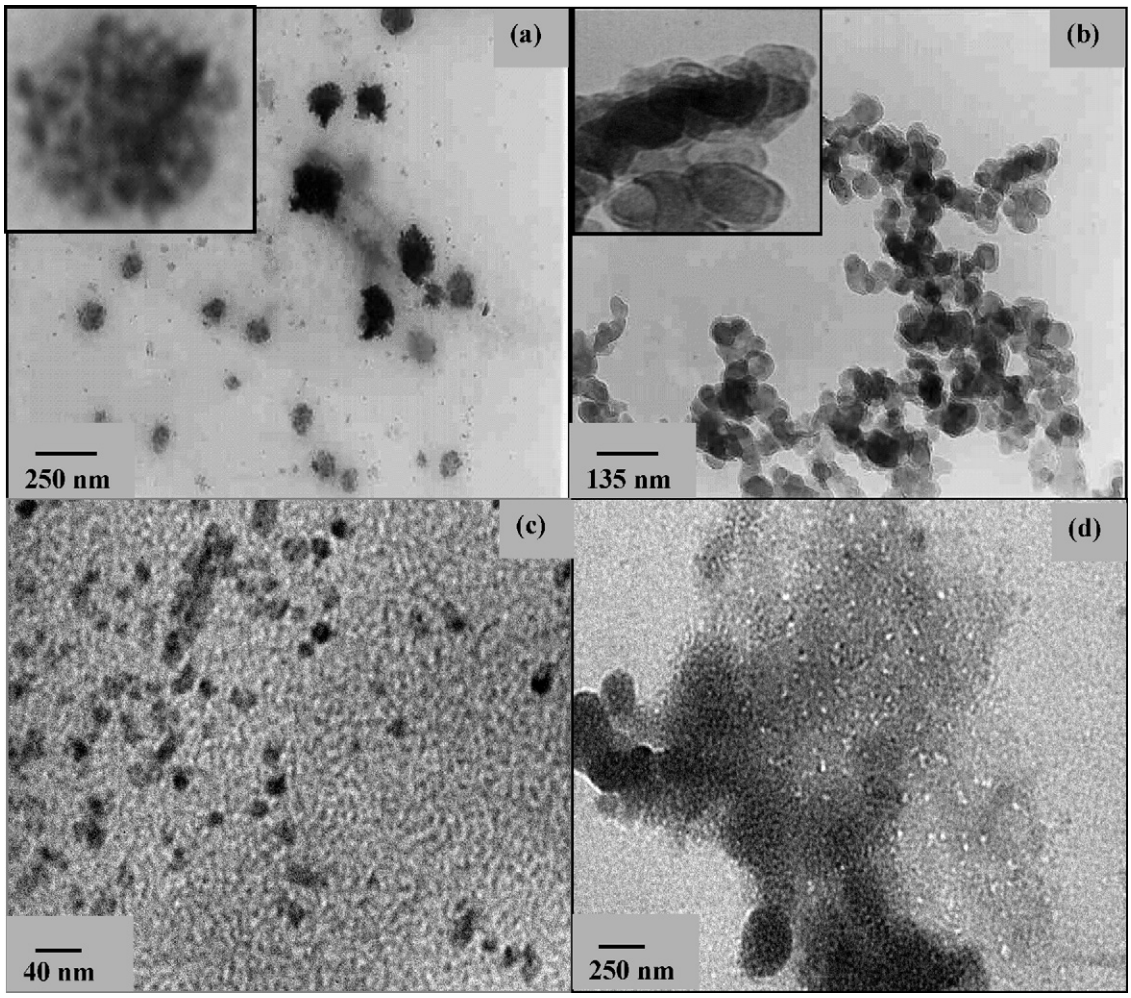

Fig. 2. TEM micrographs of CdSe nanocrystals with different precursor Cd/Se ratios; (a) 0.5:1; (b) 2:1; (c) and (d) are their corresponding micrographs in the presence of amine PPD (~1 mM), respectively. The insets on the left hand side of (a) and (b) represent the magnified portion of the selected areas.

Since the oxidation potential of PPD is 0.26 V vs. NHE, it can effectively scavenge the photogenerated holes from the CdSe surface which results in a decrease in emission yield and hence higher PL quenching efficiency is expected [21]. On the other hand, since the oxidation potentials of TEA and aniline being 0.66 and >1.0 V [21], respectively, which is more than the oxidation potential of PPD (0.26 V), the lesser quenching efficiency of the former as compared to the later can thus be understood.

In the simplest case of collisional quenching, the following relation (1), called the Stern–Volmer equation [22] hold:

$$\frac{I_0}{I} = 1 + K_{SV}[Q] \quad (1)$$

where I_0 and I are the fluorescence intensities observed in the absence and presence, respectively, of quencher, [Q] is the quencher concentration and K_{SV} is the Stern–Volmer quenching constant. In the simplest case, then a plot of I_0/I vs. [Q] should yield a straight line with a slope equal to K_{SV} [22]. Such a plot known as a Stern–Volmer plot is shown in Fig. 4(A) (curves a–c) for the case of quenching of fluorescence of 14 nm CdSe nanocrystallite with different amines [PPD, TEA and aniline]. However, as evident from Fig. 4(A) (a–c), non-linear Stern–Volmer plots with negative deviation from linearity are obtained. Such non-linear Stern–Volmer plots can occur in the case of collisional or static quenching if some of the fluorophores are less accessible than the others [22,23]. Thus in the case of Stern–Volmer plot (Fig. 4(A) (a)), of CdSe nanocrystallite (size ~14 nm) and PPD, two-population of fluorophores are present, one being accessible to quencher (PPD) and the other inaccessible or buried. From Fig's 4(A) (curves b, c) for 14 nm CdSe nanocrystallite, the similarity in the Stern–Volmer plots for TEA and aniline with PPD clearly indicates the presence of heterogeneous quenching due to the presence of accessible and inaccessible set of fluorophores, respectively. The heterogeneous quenching could be as a result of insufficient coverage of amines on the larger nanocrystallites (size ~14 nm) surface. This fractional accessibility has also been observed with the iodide quenching of tryptophan residues [22,23].

The total fluorescence emission intensity in the absence of quencher is given by

$$I_0 = I_0^a + I_0^b \quad (2)$$

where the subscript (0) refers to the florescence intensity in the absence of quencher. In the presence of quencher, Q, the intensity of the accessible fraction, I^a, is decreased in the usual Stern–Volmer manner, i.e., Eq. (1), whereas the buried fraction (I^b) is unquenched [24,25]. Therefore, the observed fluorescence intensity, I is given by

$$I = \frac{I_0^a}{1 + K_{SV}[Q]} + I_0^b \quad (3)$$

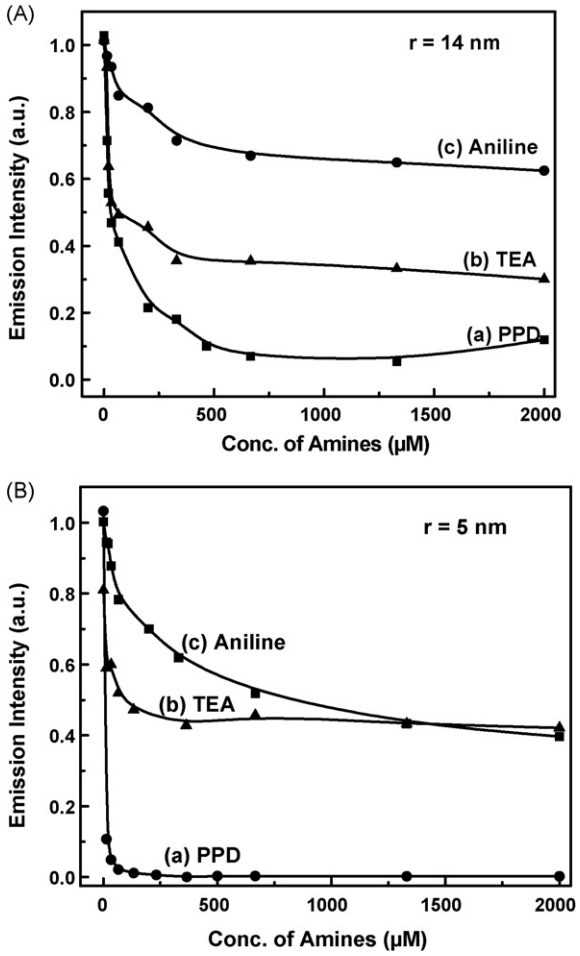

Fig. 3. Emission intensity profiles of CdSe nanocrystals of size (r) (A) 14 and (B) 5 nm in the presence of amines at different concentrations; (a) PPD; (b) TEA and (c) aniline.

where K_{SV}^{a} is the Stern–Volmer quenching constant of the accessible fraction. Subtraction of Eq. (3) from Eq. (1) gives

$$\Delta I = I_0 - I = \frac{I_0^{a}(K_{SV}^{a}[Q])}{1 + K_{SV}^{a}[Q]} \tag{4}$$

Inversion of Eq. (4) followed by its division into Eq. (2) gives

$$\frac{I_0}{\Delta I} = \frac{1}{f_a K_{SV}^{a}[Q]} + \frac{1}{f_a} \tag{5}$$

Here f_a is the fraction of the initial florescence which is accessible to quencher, where

$$f_a = \frac{I_0^{a}}{I_0^{a} + I_0^{b}} \tag{6}$$

Hence, this modified form of the Stern–Volmer equation allows for K_{SV}^{a} and f_a to be determined graphically. A plot of $I_0/\Delta I$ against $1/[Q]$ gives the gradient as $1/f_a K_{SV}^{a}$ and the intercept as $1/f_a$. The intercept represents the extrapolation to infinite quencher concentration, i.e., $1/[Q] = 0$. The value of $I_0/(I_0 - I)$ at this quencher concentration, therefore, represents the fluorescence which is quenched and only the inaccessible buried fluorophore will be fluorescent.

Fig. 4(B) (curves a–c) shows a modified Stern–Volmer plot of $I_0/\Delta I$ vs. $1/[Q]$ for CdSe nanocrystallite of size ~14 nm. Here, $[Q]$ represents the concentration of amines [PPD, TEA and aniline]. As shown in Fig. 4(B) (a–c), linear Stern–Volmer plots are obtained but for PPD and TEA case, linearity was observed only for low values of $1/[Q]$ whereas for aniline, linearity was obtained throughout the range.

From Fig. 4(B) (curves a–c) from the intercept and the gradient, the values of accessible fraction of fluorophores (f_a) is found to be 0.91, 0.58 and 0.39 and the corresponding values for Stern–Volmer quenching constant (K_{SV}^{a}) as 4×10^{-2}, 1.5×10^{-2} and 0.9×10^{-2} for PPD, TEA and aniline amines, respectively.

Fig. 4(C) (curves a–c) shows a Stern–Volmer plot for the quenching of fluorescence of 5 nm CdSe nanocrystallite with different amines [PPD, TEA and aniline]. As observed in Fig. 4(B), here also non-linear Stern–Volmer plots (−ve deviation from linearity) are obtained indicating the presence of heterogeneous quenching (Fig. 4(C)) for different amines. From Fig's 4(A and C) (curves a), it is evident that the linear portion of the Stern–Volmer plot for smaller CdSe crystallite extends up to 500 μM concentration as compared to only 30 μM of PPD corresponding to larger crystallite size ~14 nm. Thus, due to smaller nanocrystallite size ~5 nm and hence less steric hindrance, PPD coverage is enough on the surface to ensure the presence of maximum number of accessible fluorophores as compared to the corresponding case for larger ~14 nm CdSe nanocrystallite size.

PPD owing to its lower oxidation potential (~0.26 V) has a stronger quenching action and hence extended linearity up to higher concentration in Stern–Volmer plots are observed as compared to amines having higher oxidation potential of 0.66 and >1.0 V for TEA and aniline particularly for smaller CdSe nanocrystallites, respectively.

Fig. 4(D) (curves a–c) shows the modified Stern–Volmer plots ($I_0/\Delta I$ vs. $1/[Q]$) for different amines corresponding to smaller CdSe nanocrystallite (~5 nm). Here, these modified Stern–Volmer plots are found to be similar as observed in the case of larger CdSe nanocrystallite as well. From Fig. 4(D) (curves a–c), the values of accessible fraction of fluorophores (f_a) is found to be 1.0, 0.63 and 0.52 and the corresponding values for Stern–Volmer quenching constant (K_{SV}^{a}) as 7.2×10^{-2}, 1.4×10^{-2} and 3.3×10^{-2} for PPD, TEA and aniline amines, respectively. It is interesting to note that for smaller nanocrystallite size, there is an increment in the number of the accessible fraction of fluorophores and higher rate constants are observed as compared to that of larger CdSe nanocrystallite. This effect is felt more for PPD essentially due to its lower oxidation potential as compared to other amines TEA and aniline, respectively.

From above, it is still not clear about the type of quenching mechanism (static or dynamic) present for both smaller and larger sized CdSe nanocrystallites. If the quenching process arises from binding between the fluorophore and the quencher (static quenching), then regardless of the population of the inaccessible fluorophores, a plot of $I_0/\Delta I$ vs. $1/[Q]$ is linear. However, if the modified Stern–Volmer plots are not linear, then it may be concluded that binding processes, if they occur, are not the dominant mechanisms for the quenching of the fluorescence [22,26]. In our case for both smaller and larger CdSe nanocrystallites, except for the aniline case where the modified Stern–Volmer plots are absolutely linear throughout the range of $1/[Q]$, for other amines like PPD and TEA, the modified Stern–Volmer plots show linearity only for lower values of $1/[Q]$. Hence, for PPD and TEA, static quenching does not seem to be the dominant one for CdSe nanocrystallites of varied sizes. Other quenching process like dynamic or collisional may be responsible for the quenching of CdSe fluorophores with the quencher, i.e., amines [PPD and TEA].

From above Stern–Volmer plots, it is clear that the fluorescence quenching data alone cannot distinguish clearly between dynamic or static processes. Additional information is required to distinguish between the two; for example, the temperature-dependence and

lifetime measurements [22,27]. An increase in temperature leads to an increase in the diffusion constant of quencher and will generally lead to an increase in collisional quenching [22,27]. In contrast, an increase in temperature will generally lead to a decrease in the binding constant of quencher for fluorophore and will result in a decrease in quenching for a static quencher [22,27]. In the case of static quenching, only fluorophore intensity reduces with quencher concentration while the lifetime of the excited species remains unperturbed and thus $\Gamma_0/\Gamma = 1$ where Γ_0 and Γ are the lifetimes of the excited species in the absence and presence of quencher, respectively. However, in case of dynamic or collisional quenching, both fluorescence intensity and the lifetime decreases with quencher concentration and is related to Stern–Volmer plot as $I_0/I = \Gamma_0/\Gamma$ [22,27].

Fig. 5(A–C) shows temperature-dependence of Stern–Volmer plots for different amines [PPD, TEA and aniline] for a smaller (size ~5 nm) CdSe nanocrystallite. As shown in Fig. 5(A) (curves a–c), with increase in temperature from 25 to 80 °C, the ratio of I_0/I increases with PPD concentration, thus indicating an increase in collisional quenching. Similar feature can also be observed in the case of TEA (Fig. 5(B) (curves a–c)). However, from Fig. 5(C) (curves a–c)), in the case of aniline, the ratio I_0/I decreases with increase in temperature in sharp contrast to that of obtained for PPD and TEA amines. This is indicative of a static quenching process where an increase in temperature results in decrease in stability and subsequent break-up of the non-fluorescent ground state complexes.

In order to further probe the interaction between CdSe and amines [PPD, TEA and aniline], the fluorescence decay was monitored using 337 nm laser pulse as the excitation process. As shown in Fig. 6(A–C) for different amines, the emission intensity recorded at the emission maximum exhibited a multiexponential decay and

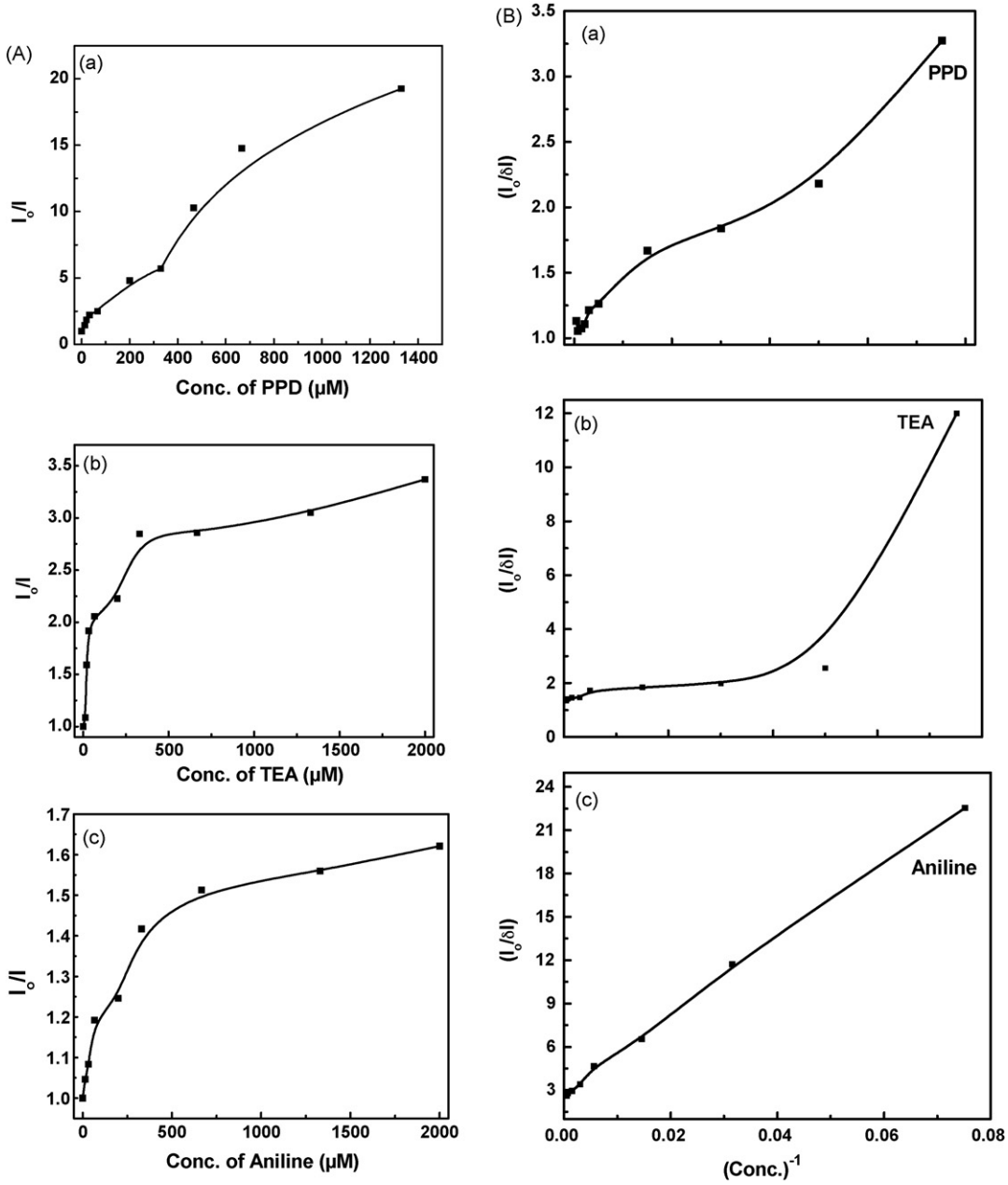

Fig. 4. Stern–Volmer plots (I_0/I vs. concentration of amines) of CdSe/amines system for CdSe nanocrysallites of size (A) 14 and (C) 5 nm; (a) PPD; (b) TEA and (c) aniline. (B) and (D) are their corresponding modified Stern–Volmer plots ($I_0/\Delta I$ vs. inverse of concentration of amines).

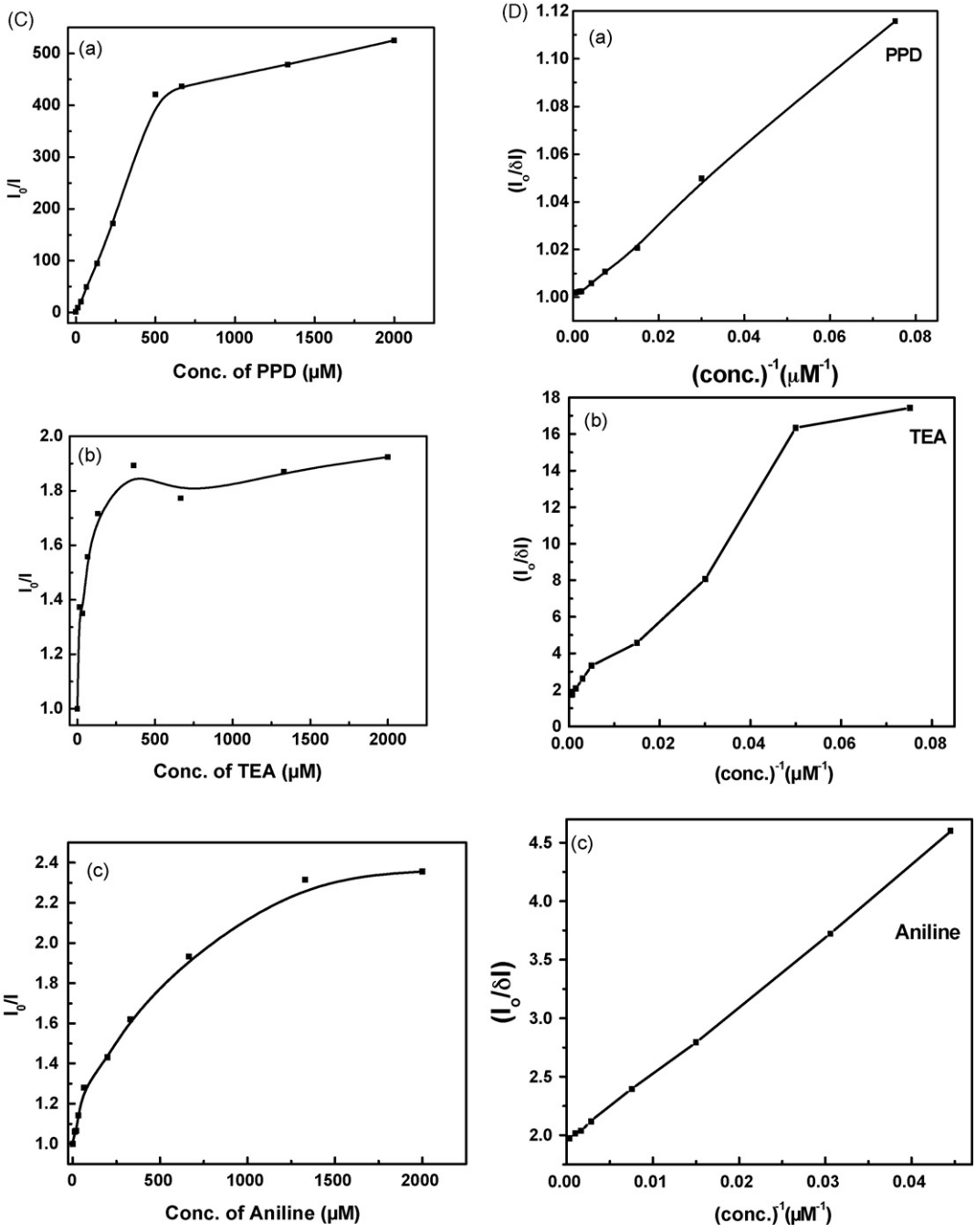

Fig. 4. (*Continued*)

was analyzed using the expression (7) [28].

$$F(t) = a_1 \exp\left(\frac{-\Gamma}{\Gamma_1}\right) + a_2 \exp\left(\frac{-\Gamma}{\Gamma_2}\right) + a_3 \exp\left(\frac{-\Gamma}{\Gamma_3}\right) \quad (7)$$

We have determined an average emission lifetime Γ_{avg} for CdSe emission by using an expression (8) described by James et al. [29] for the emission from solid surfaces,

$$\Gamma_{avg} = \frac{(a_1\Gamma_1 + a_2\Gamma_2^2 + a_3\Gamma_3^2)}{(a_1\Gamma_1 + a_2\Gamma^2 + a_3\Gamma_3)} \quad (8)$$

Fig. 7(A) (a–c) shows a plot of average lifetime of the charge carriers of CdSe quantum dots of size ~5 nm with amines [PPD, TEA and aniline] concentration. As evident from Fig. 7(A) (c), in the case of aniline we observe little variation in the average lifetimes ~58 ns up to 1330 μM although decrease in the emission yield of CdSe nanocrystallites with increasing concentrations of aniline has been observed but it has little effect on the emission decay behavior. On the other hand, the decrease in the average lifetime observed with increasing PPD and TEA concentrations parallels the decrease observed in emission yield. For 5 nm diameter CdSe nanocrystallite, we observe a decrease in average lifetime from ~61 to ~41 ns for PPD and to ~30 ns for TEA as we increase the amines [PPD, TEA] concentration from 0 to 1 mM.

Thus from above, the increase in I_0/I with increase in temperature and decrease in lifetime values with increase in concentrations of amines [PPD, TEA] suggests that dynamic quenching is essentially

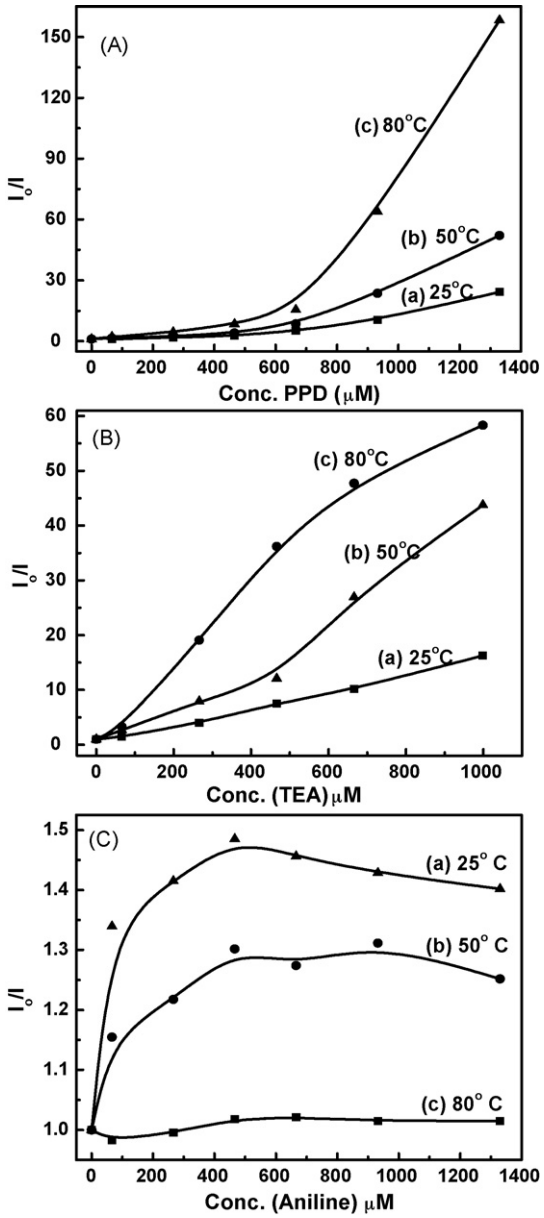

Fig. 5. Stern–Volmer plots (I_0/I vs. concentration of amines) of CdSe/amines system for CdSe nanocrysallites of size 5 nm at different temperatures; (A) PPD; (B) TEA and (C) aniline; (a) 25 °C; (b) 50 °C and (c) 80 °C.

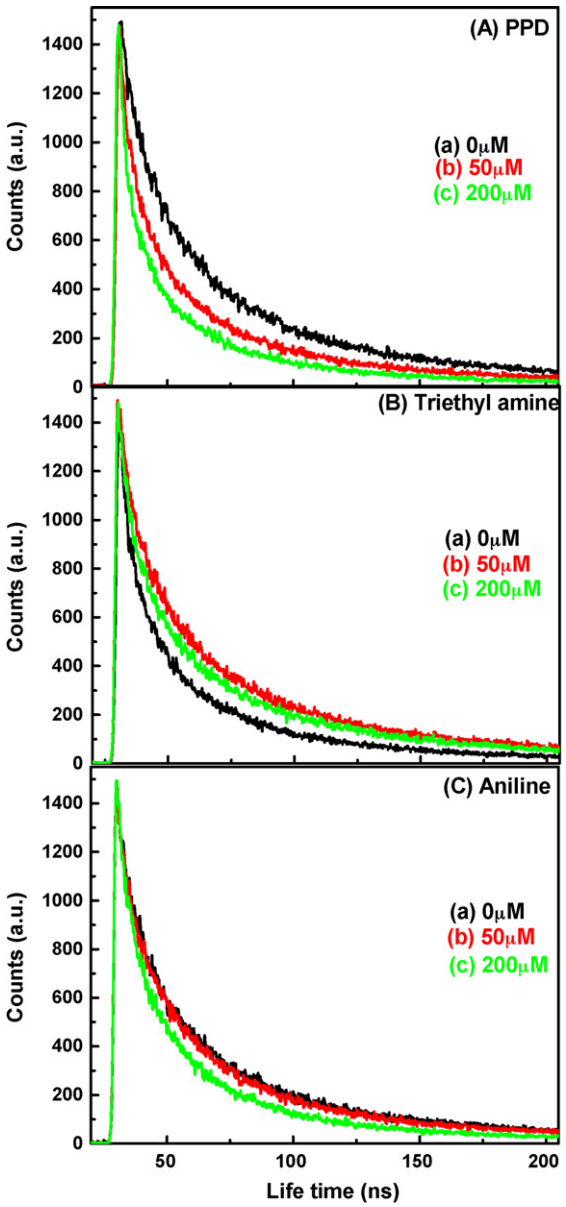

Fig. 6. Emission decay of CdSe–amines system for CdSe quantum dots of size 5 nm at different concentrations of amines; (A) PPD; (B) TEA and (C) aniline; (a) 0 μM; (b) 50 μM and (c) 200 μM.

responsible for the decrease in emission yield of CdSe nanocrystallites. On the other hand, I_0/I decreases with increase in temperature and the lifetime values remain nearly unchanged with increase in concentration of aniline amines which suggests that static quenching is the dominant mechanism. Furthermore, there is an increase in rate constant k_q with temperature as observed in the case of PPD and TEA indicating dynamic or collisional quenching to be the dominant mechanism. However, in the case of aniline, there is a decrease in the rate constant (k_q) with temperature, which suggests that static quenching is mainly responsible for the decrease in emission yield for CdSe nanocrystallites. For collisional quenching, from the Stern–Volmer plot of I_0/I vs. [Q], gradient = $K_{SV} = k_q\,\Gamma_0$ (Γ_0 = ~60 ns for pure CdSe), the value of rate constant k_q, hence can be calculated. From Fig. 7(B) (a–c), a plot of Γ_0/Γ vs. [Q] yields a straight line for aniline (static quenching) and a linear curve for PPD and TEA amines (dynamic quenching) further supports the above theory. When aniline is added to CdSe nanoparticles of size ~5 nm, the amine binds to the nanoparticle surface by serving as hole trap, thereby removing these sites from participation in radiative electron–hole recombination on the surface. In this way, aniline quenches the fluorescence of CdSe nanocrystallites without changing its lifetime.

In order to probe the charge transfer across CdSe-amines, FTIR transmittance spectra of CdSe nanocrystallite (size ~5 nm) in the absence and presence of PPD and aniline amines were taken. The amines with lowest (~0.26 V) and highest (>1.0 V) oxidation potentials, i.e., PPD and aniline were chosen, respectively. Fig. 8(a) shows the FTIR transmittance spectra of pure CdSe (without amines) and it exhibits well-defined main peaks: triplet band between 2880–3100 cm^{-1}, 2360 cm^{-1} and 725 cm^{-1} corresponding to CH-stretching (sp^3), CH-bending and methylene ($-CH_2$) vibrational modes, respectively [30,31]. However, the presence of strong IR peak at ~1490 cm^{-1} with a shoulder at 1467 cm^{-1} corresponding to P=O stretching vibrational modes indicates the signatures

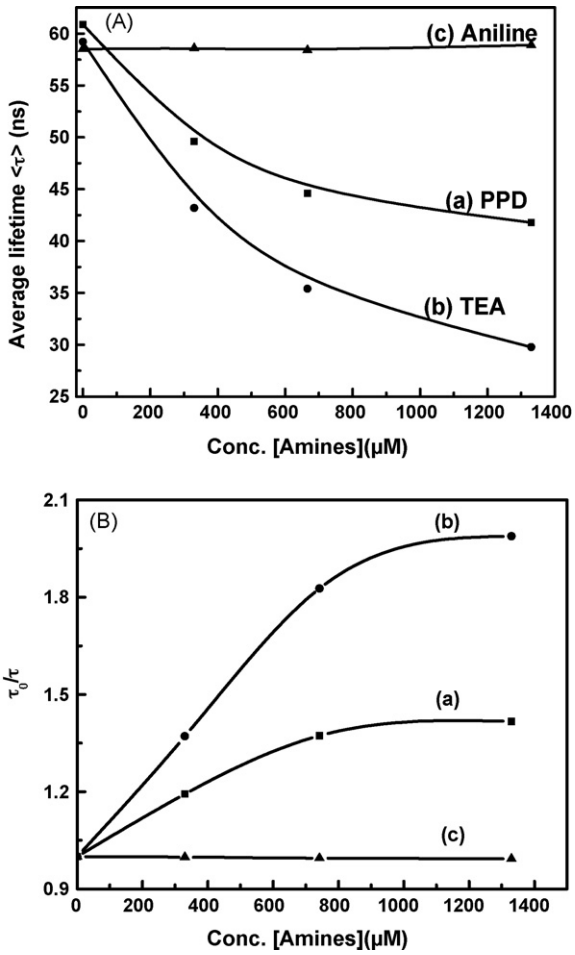

Fig. 7. Average lifetimes ⟨τ⟩ (A) and ratio of τ_0/τ (B) of 5 nm CdSe quantum dots in the presence of amines; (a) PPD; (b) TEA and (c) aniline.

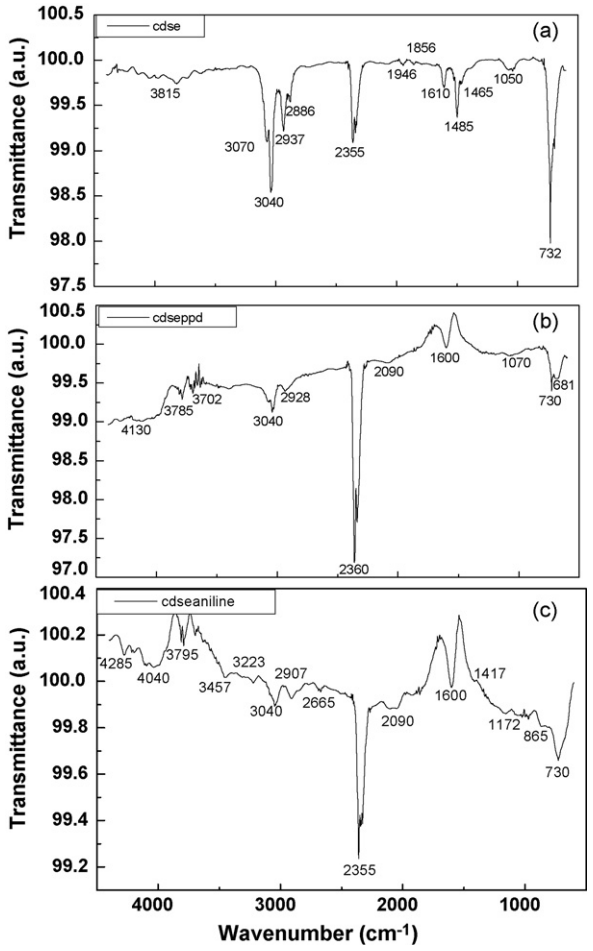

Fig. 8. FTIR spectra of (a) CdSe nanocrystals of size 5 nm; (b) CdSe–PPD system and (c) CdSe–aniline system. Here, concentrations of PPD and aniline being 2 mM.

of capping agent, i.e., TOPO/TOP bounded to CdSe nanocrystals, respectively [31]. In the presence of amines PPD and aniline, the signature of TOPO/TOP transmittance signal vanishes completely for PPD (Fig. 8(b)) while for aniline, it corresponds to a weak signal at ∼1417 cm^{-1} (Fig. 8(c)). Since the oxidation potential of PPD is 0.26 V vs. NHE, it can effectively scavenge the photogenerated holes from the CdSe surface. On the other hand, the oxidation potential of aniline is >1.0 V vs. NHE which in turn makes it ineffective as scavenger of photogenerated holes as compared to PPD. The fluorescence quenching and lifetime measurements also points out the higher quenching efficiency of PPD as compared to TEA and aniline for CdSe nanocrystallites of varied sizes.

We will now consider butyl amine (primary aliphatic) which has the maximum of oxidation potential (>1.9 V) [21] amongst all other amines studied so far. It would be interesting to investigate the effect of butyl amine on the fluorescence intensity of CdSe nanoparticles of varied sizes. As shown in Fig. 9(A and B), with the increase in butyl amine concentration from 0 to 2 mM, the emission yield of 14 nm CdSe nanocrystallite increases. At concentrations around 1 mM, the emission yield of CdSe system saturates (Fig. 9(B)). At these concentration levels most of the CdSe particle surface is complexed with butyl amine. The fact that the emission maximum and spectral shape are independent of butyl amine concentration rules out formation of new surface states. The enhancement in the emission intensity of CdSe system in the presence of butyl amine could be due to the binding of butyl amine to low energy (surface defect sites) on CdSe surface which results in saturation of electron trapping sites and thus promotes radiative decay. However, in the case of 5 nm CdSe nanocrystallite, we see a quenching of the emission (Fig. 10(A and B)). Here, nearly all the emission from CdSe quantum dots is quenched at the concentration level of 2 mM. Our results of decrease in fluorescence emission intensity of CdSe system with butyl amine is in accordance with M.A. El-Sayed group [4,32] which observed quenching in emission intensity of CdSe nanoparticles upon interaction with butyl amine. Thus the interaction of butyl amine with CdSe surface is an artifact of the size of CdSe quantum dots. For smaller CdSe nanocrystallite (∼5 nm), it acts as an efficient quencher and for larger CdSe nanocrystallite (∼14 nm), it enhances the emission yield. Since the oxidation potential of PPD is 0.26 V vs. NHE, it can effectively scavenge the photogenerated holes from the CdSe surface and resulting in a decrease in emission yield as observed in the case of smaller and larger CdSe nanocrystallites, respectively. It is important to note that the valence band-edge of CdSe quantum dot is expected to be around +1.2 V vs. NHE [33]. Moreover, the size quantization effect and surface-bound ligands are expected to shift the valence band to more positive potentials, thus making it a stronger oxidant than the bulk [33]. However, this shift in valence band is likely to be ≤0.5 V and is not sufficient to oxidize butyl amine. In addition, oxidation potential of butyl amine is >1.9 V vs. NHE, and thus it is not expected to act as an effective scavenger of photogenerated holes like PPD. However, experimentally it has been observed that for smaller CdSe quantum dots (∼5 nm), butyl amine is a strong quencher. Thus it seems that the oxidation potential of amines particularly butyl amine are dependent on the

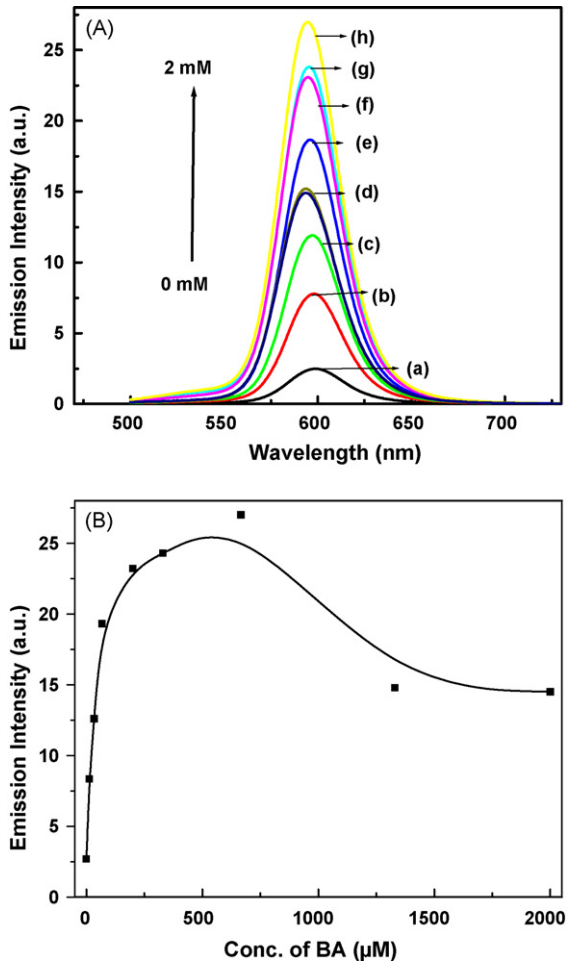

Fig. 9. Emission intensity profiles (A) and (B) of TOPO-capped CdSe nanocrystals of size 14 nm in the presence of butyl amine at different concentrations; (a) 0, (b) 0.1, (c) 0.2, (d) 0.3, (e) 0.4, (f) 0.6, (g) 1.2 and (h) 2 mM, respectively.

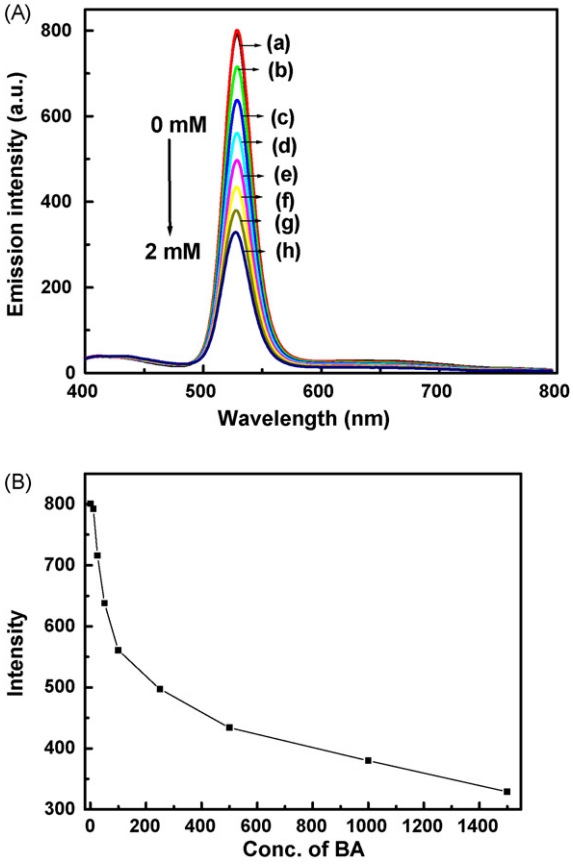

Fig. 10. Emission intensity profiles (A) and (B) of TOPO-capped CdSe nanocrystals of size 5 nm in the presence of butyl amine at different concentrations; (a) 0, (b) 0.1, (c) 0.2, (d) 0.3, (e) 0.4, (f) 0.6, (g) 1.2 and (h) 2 mM, respectively.

size of the quantum dots. This is in accordance with observation of Sionnest and coworkers [34] which reported an ensemble reduction potential of amines for three different sized quantum dots. Furthermore, Sionnest and coworkers [34] had noted that there are easily 0.2 V changes of the oxidation potential depending on what sort of ligand passivates the surface of the dot. On the basis of the above argument, the role of butyl amine in enhancing and decreasing the emission yield of varied sized CdSe quantum dots can be explained.

From above studies of quenching of CdSe nanocrystallites particularly the smaller ones by different amines [PPD, TEA, aniline, BA], it has been found that steric factors play a role in their quenching abilities. A tertiary amine showed reduced quenching efficiency, compared to the secondary and primary amines. The results can be explained by the restricted diffusion of a bulky amine through the CdSe network. TEA and butyl amines though both being aliphatic amines, but their quenching efficiency differs. TEA being a bulkier amine has a weaker quenching ability as compared to smaller butyl amine as observed in the case of smaller CdSe nanocrystallites (size ~5 nm). Although smaller butyl amine has slightly less basicity (electron-donating ability) and higher oxidation potential as compared to bulkier TEA, the former has a stronger quenching ability than the latter [35,36]. Although PPD because of its ring structure, the adsorption on the particle surface should be less favorable on geometric grounds but in our study, the diamine (PPD) shows a higher quenching ability presuming due to its lowest oxidation potential as it has the highest electron-donating ability, i.e., it can readily scavenge the photogenerated holes from the CdSe surface as evident from reactions (1) and (2). Aniline has the weakest electron-donating ability and thus has less basicity as compared to all other amines studied in this work, hence its weaker quenching ability can be understood. Thus on the basis of detailed studies on fluorescence quenching of CdSe nanocrystallites of different sizes by different amines, it appears that the quenching efficiency of the amines depends on the complex combination of oxidation potential, crystallite sizes and steric factors.

4. Conclusions

The interaction of aliphatic (triethyl amine, butyl amine) and aromatic amines (*p*-phenyline diamine (PPD), aniline) with CdSe quantum dots of smaller (~5 nm) and larger (~14 nm) sizes is reported. It has been found that steric factors play a role in the quenching abilities of different amines. Smaller quantum dots facilitate better surface coverage of amines and thus higher quenching efficiency of amines could be realized as compared to larger CdSe quantum dots. The quenching efficiency in general follows the trend: $PL_{quenching}$ (PPD) ≫ $PL_{quenching}$ (TEA) > $PL_{quenching}$ (aniline). The beneficial effect of butyl amine in enhancing the emission of larger CdSe quantum dots upon its post-synthesis addition has been explored. It is presumably due to the enhanced capping effect and thus realization of better passivation of surface-traps. The changes in the emission properties and lifetime values of CdSe quantum dots arising from the interactions with different amines are greatly

influenced by a combination of oxidation potential of amines and crystallite sizes.

Acknowledgements

We thank Director NPL for the encouragement to perform this work. The financial assistance from Department of Science and Technology, New Delhi is gratefully acknowledged. Dr. Nirmalaya Karar and Dr. Harish Chandra (Luminescent Materials and Phosphors Group, NPL, Delhi) are acknowledged for their help in Photoluminescence (PL) measurements.

References

[1] J.A. Gaunt, A.E. Knight, S.A. Windsor, V. Chechik, J. Colloid Interf. Sci. 290 (2005) 437.
[2] S. Coe, W.K. Woo, M.G. Bawendi, V. Bulovi, Nature 420 (2003) 800.
[3] M. Bruchez, M. Moronne, P. Gin, S. Weiss, A.P. Alivisatos, Science 281 (1998) 2019.
[4] C. Landes, C. Burda, M. Braun, M.A. El-Sayed, J. Phys. Chem. B 105 (2001) 2981.
[5] C.J. Murphy, Anal. Chem. 74 (2002) 521A.
[6] X. Peng, L. Manna, W. Yang, J. Wickham, E. Scher, A. Kadavanich, A.P. Alivisatos, Nature 404 (2000) 59.
[7] D. Gerion, F. Pinaud, S.C. Williams, W.J. Parak, D. Zanchet, S. Weiss, A.P. Alivisatos, J. Phys. Chem. B 105 (2001) 8861.
[8] I. Sondi, O. Siiman, E. Matijevic, J. Colloid Interf. Sci. 275 (2004) 503.
[9] L. Spanhel, M. Haase, H. Weller, A. Henglein, J. Am. Chem. Soc. 109 (1987) 5649.
[10] M.Y. Gao, S. Kirstein, H. Mohwald, A.L. Rogach, A. Kornowski, A. Eychmuller, H. Weller, J. Phys. Chem. B 102 (1998) 8360.
[11] M.A. Hines, P. Guyot-Sionnest, J. Phys. Chem. 100 (1996) 468.
[12] M. Danek, K.F. Jensen, C.B. Murray, M.G. Bawendi, Chem. Mater. 8 (1996) 173.
[13] H. Mattaoussi, A.W. Cumming, C.B. Murray, M.G. Bawendi, R. Ober, J. Chem. Phys. 105 (1996) 9890.
[14] S.N. Sharma, Z.S. Pillai, P.V. Kamat, J. Phys. Chem. B 107 (2003) 10088.
[15] G.C. Lisensky, R.L. Penn, C.J. Murphy, A.B. Ellis, Science 248 (1990) 840.
[16] N. Chandrasekharan, P.V. Kamat, Res. Chem. Intermed. 28 (2002) 847.
[17] Shailesh N. Sharma, H. Sharma, G. Singh, S.M. Shivaprasad, Nucl. Inst. Meth. Phys. Res. B 244 (2006) 86.
[18] H. Sharma, Shailesh N. Sharma, G. Singh, S.M. Shivaprasad, Physica E 31 (2006) 180.
[19] P.A. Sant, P.V. Kamat, Phys. Chem. Chem. Phys. 4 (2002) 198.
[20] J.H. Adair, T. Li, T. Kido, K. Havey, J. Moon, J. Mecholsky, A. Morrone, D.R. Talham, M.H. Ludwig, L. Wang, Mater. Sci. Eng. R 23 (1998) 139.
[21] R.C. Weast, Handbook of Chemistry and Physics, 54th ed., CRC Press, 1973.
[22] J.R. Lakowicz, Principles of Fluorescence Spectroscopy, 2nd ed., Kluwer-Plenum, New York, 1999.
[23] C.M. Samworth, M.D. Esposti, G. Lenaz, Eur. J. Biochem. 171 (1988) 81.
[24] S.S. Lehrer, Biochemistry 10 (1971) 3254.
[25] W.A. Wyatt, F.V. Bright, G.M. Hieftje, Anal. Chem. 59 (1987) 2272.
[26] K.R. Thulburn, W.H. Sawyer, Biochem. Biophys. Acta 511 (1978) 125.
[27] J.B. Birks (Ed.), Organic Molecular Photophysics, Wiley, New York, 1975, p. 409.
[28] C.F. Landes, M. Braun, M.A. El-Sayed, J. Phys. Chem. B105 (2001) 10554.
[29] D.R. James, Y.-S. Liu, P. de Mayo, W.R. Ware, Chem. Phys. Let. 120 (1985) 460.
[30] G.B. Deacon, J.H.S. Green, Spectrochim. Acta 24a (1968) 845.
[31] L.R. Becerra, C.B. Murray, R.G. Griffin, M.G. Bawendi, J. Chem. Phys. 100 (1994) 3297.
[32] M.A. El-Sayed, Acc. Chem. Res. 37 (2004) 326.
[33] J. Hu, L. Li, W. Yang, L. Manna, L.-W. Wang, A.P. Alivisatos, Science 292 (2001) 2060.
[34] C. Wang, M. Shim, P. Guyot-Sionnest, Science 291 (2001) 2390.
[35] W. Kemp, Organic Spectroscopy, third ed., ELBS, McMillan, London, 1991.
[36] B.R. Chandler-Henderson, B. Sweryda-Krawiec, J.L. Coffer, J. Phys. Chem. 99 (1995) 8851.